RSC Advances

This article can be cited before page numbers have been issued, to do this please use: W. Huang, H. Zhu, Y. L. Huang, J. W. Yang and W. Wang, *RSC Adv.*, 2016, DOI: 10.1039/C6RA05709H.

ROYAL SOCIETY OF CHEMISTRY

www.rsc.org/advances

View Article Online
DOI: 10.1039/C6RA05709H

Journal Name

RSCPublishing

ARTICLE

Controllable Synthesis of Conjugated Thiophenylethyne-based Compounds with Different Chain Lengths

Cite this: DOI: 10.1039/x0xx00000x

Received 00th January 2012,
Accepted 00th January 2012

DOI: 10.1039/x0xx00000x

www.rsc.org/

Wei Huang,[a] Haoyun Zhu,[a] Yuli Huang,[a] Junwei Yang,[a] and Weizhi Wang*[a]

Thiophenylethyne-based compounds have been extensively investigated for some molecular electronic devices. Based on thiophene and acetylene units, a series of oligomers and polymer owning different chain lengths were designed and synthesized via Sonogashira reaction in this work. These compounds were characterized by some routine measurements to demonstrate that the optical bathochromic shifts and decreasing band gaps were caused by the increasing conjugated backbones. Meanwhile, synchrotron-based two-dimensional grazing-incidence X-ray diffraction was adopted to study the molecular stacking orientations with respect to the surfaces. The closer distance between the lamellar layers was testified to be a contribution to the better conducting property of the compounds. Moreover, the microscopic structural study directly provided further explanation for the good performance of the polymer in this system. Some top-gate field-effect transistors via solution processing were fabricated with the selected oligomers and the polymer. And the polymer devices showed nice performance of charge transport mobility at 0.42 $cm^2V^{-1}s^{-1}$ with an on-off ratio of 1.59×10^3, which were much better than those of the oligomers.

1. Introduction

Since the discovery of conducting polyacetylene, conducting polymers, a class of polymers permitting delocalized charge carriers transport with a sp^2 structure, have been a popular researching field in the material study.[1-6] A lot of new conducting polymers are stimulated to be synthesized by their possible applications like sensors, organic photovoltaics, super capacitors, organic light-emitting diodes, batteries, and so forth.[7–11] Among the enormous studies, some p-conjugated oligomers and polymers have been widely investigated for fabricating molecular electronics.[12-14] Actually, oligo- and polythiophenes are considered to be one of the best candidates for applying to the components of electronic devices,[15-18] because some highly electronic conductive composites would be produced by the oxidation of oligo- and polythiophenes. A classic example is the research of poly(3-alkylthiophenes) (P3AT) family in recent years, due to their good solubility, wide availability, environmental stability and ease of processing from the solutions into the solid thin-films.[19-22]

Apart from the well-studied P3AT, the studies of other interesting conducting compounds with π-expanded conjugation, poly(2,5-thienylene ethynylene) (**PTE**), seem to be little in the field of conducting materials. This kind of polymer with low molecular weight only consisting of alternating acetylene and thiophene units was first reported by D. L. Trumbo in 1986.[23] Since then, a few scientists have devoted to the relevant work of these related compounds, including linear type and macrocyclic type. In the early days, Michael P. Cava and Takakazu Yamamoto[24-25] have worked on improving routines to synthesize **PTE** with higher molecular weight or the preparation of some regiocontrolled polymers. Ronald Breslow[26] synthesized and examined a family of molecular wires consisting of oligothiophenes and oligothiophenylethynes for the construction of the molecular field-effect transistors (FETs). Giant macrocyclic oligomers with 60π-180π electron systems, only composed of thiophene and acetylene units, were synthesized by Masahiko Iyoda via McMurry coupling reaction.[27] At the same time, the ordered self-assembly and aggregation structure on the surface of the acetylene-based oligomers and polymers have received only limited attention. Trolle R. Linderoth and Kurt V. Gothelf used scanning tunneling microscopy (STM) to study the self-assembly of several designed oligo(naphthylene-ethynylene) molecular rod molecules when adsorbed on the surfaces.[28] Yufeng Lu studied the formation and self-assembly behavior of conjugated **PTE**/silica nanocomposites.[29] The π-conjugated structure of **PTE** showed its potential to be applied in electronic devices like FETs, which were composed of a substrate, a semiconductor, drain-source electrodes, a

[a] *State Key Laboratory of Molecular Engineering of Polymers, Collaborative Innovation Center of Polymers and Polymer Composite Materials, Department of Macromolecular Science, Fudan University, Shanghai 200433, P. R. China.*
** Corresponding Author*
E-mail: weizhiwang@fudan.edu.cn. Tel: +86 021-65643836
† *Electronic supplementary information (ESI) available. See DOI: 10.1039/cxxxxxxxxx*

View Article Online
DOI: 10.1039/C6RA05709H
Journal Name

dielectric layer and a gate electrode.[30] Masahiko Iyoda and his co-workers[31] just reported on the surface structures and FET behavior of macrocyclic oligothiophene with 6-mers. And their FETs containing the π-π stacking oligomers showed a good on-off ratio of 10^4, but with a low charge carrier mobility of 2.8 x 10^{-3} $cm^2V^{-1}s^{-1}$.

According to the references, **PTE** attracted our attention because of their interesting properties and assembly behavior. Accordingly, a series of thiophenylethyne-based oligomers and polymers (**1**-**4** and **PTE**) were successfully designed and synthesized via Sonogashira reaction in this work. And they were studied by kinds of characterizations like UV absorption, photoluminescence (PL) and cyclic voltammetry (CV) to see how the increasing conjugated backbones affect the properties of the systematic compounds. In addition, we used synchrotron-based two-dimensional grazing-incidence X-ray diffraction (2D-GIXRD) to directly learn molecular stacking of the synthesized compounds. Herein, **3**, **4** and **PTE** were selected as the active semiconductor layer to fabricate some thin-film FETs, to be tested their different performance. And the molecular packing in films was utilized to provide further proof to the performance distinctions between the fabricated FETs and why these devices involving **PTE** possessed the best performance of excellent charge carrier mobility and on-off current ratios in this system.

2. Experimental details

Materials

The whole chemicals and reagents used were selected and purchased from chemical companies, J&K Scientific and Sinopharm Chemical Reagent Company. Small sodium wires and benzophenone were used to prepare dry toluene under the nitrogen (N_2) circumstance.

Measurements and Characterization

On a Bruker AVANCE III HD 400 MHz. FT-NMR spectrometer, ^1H and ^{13}C nuclear magnetic resonance spectra (NMR) were carried out in deuterated dichloromethane (CD_2Cl_2). Chemical shifts were in ppm units and tetramethylsilane (TMS; δ=0) was used as an internal standard. Gel permeation chromatography (GPC) measurements were recorded on a gel permeation chromatograph, Agilent/Wyatt 1260. The calibration was managed by employing commercially available polystyrene. A UV-visible (UV-vis) spectrophotometer, Perkin-Elmer Lambda 750 was employed for UV spectra in dichloromethane (CH_2Cl_2) solution. PL spectra were performed in CH_2Cl_2 solvent on a Photo Technology International, Inc. QM40 fluorescent lifetime spectrometers at room temperature. The PL quantum yields (Φ_F) were estimated using fluorescein (Φ_F = 92% in 0.1 M NaOH) and quinine sulfate (Φ_F = 54% in 0.1M H_2SO_4 solution) as standards. And the fluorescent lifetimes were recorded on the same QM40 spectrometers by means of a time-corrected single photon counting system at room temperature. Thermal gravimetric analysis (TGA) measurement was done with a thermo gravimetric analyzer (Perkin Elmer Pyris 1), heating from 50 to 800 °C at a heating rate of 20 °C/min, in a N_2 flow. Differential scanning calorimetry (DSC) measurement was implemented on the differential scanning calorimeter (TA Q2000), one heat-cool cycle from 50 °C to 180 °C at a ramp of 20 °C/min in a dry N_2 flow. Cyclic voltammetry (CV) was operated on one electrochemical workstation (T30/FRA2). And the glass-carbon electrolyte with a 0.08 cm^2 cross section was covered by the product films. The internal standard was ferrocene under vacuum (4.8 eV), plus 0.1 M tetrabutylammonium hexafluorophosphate ($TBAPF_6$) in acetonitrile was as the electrolyte. The measurements were performed at a scan rate of 100 mV/s under the N_2 protection. A platinum wire was the counter electrode, and $Ag/AgNO_3$ was the reference electrode. The mass spectra of the samples were analyzed by matrix assisted laser desorption ionization-time of the flight mass spectrometer (MALDI-TOF), AB SCIEX 5800. And the VARIO EL3 instrument (ELEMEN TAR, Germany) was utilized for elemental analysis. The polarizing microscope (POM) images were examined by a DM2500P polarizing microscope at room temperature. The thickness of the films formed in the FETs was measured on F40 film thickness tester. Synchrotron-based two-dimensional grazing-incidence X-ray diffraction (2D-GIXRD) was implemented at BL14B1, with the help of Shanghai Synchrotron Radiation Facility. The grazing-incidence angle was set to 0.25° and the wavelength was 0.124 nm. 0.2 wt% CH_2Cl_2 solutions of the compounds were spin-coated on the substrates for 50 s to make the samples at the rotation rate of 3500 r/m. Equipped with a Bruker SMART $_1$K CCD area detector and a rotating anode using graphite-monochromatic M_o K_α radiation (λ =0.71073 Å), a P4 Bruker diffractometer was used to collect the whole X-ray crystallographic data. A program of SAINT was for the data processing, and another program of SADABS was employed for calibrating the diffraction data. Based on the utilization of a decay correction and the redundant reflections, an empirical absorption correction was used as well. The final structure of **2** was resolved by utilizing the straight-ways procedure in the program library of Bruker SHELXL and clarified by the least-squares full-matrix approaches on F2. Some anisotropic thermal parameters were utilized to refine the non-hydrogen atoms. Simultaneously, the isotropic thermal parameters based on the bonded carbon atoms and the hydrogen atoms were combined together to calculate the positions.

FETs Fabrication.

H_2O_2/H_2SO_4, deionized water, methanol and acetone were utilized in turn to wash the commercially available SiO_2 (300 nm)/highly p-doped Si wafers. Then the clean wafers were spin-coated by the synthesized compounds, **3**, **4** and **PTE** in CH_2Cl_2 solution (0.2 wt%) at a speed of 3500 r/min. These semiconductor films were placed in a vacuum atmosphere to evaporate the surplus solvent. The thickness of the thin film in FETs was (494±2) nm. The gold drain and source electrodes (the thickness was 50 nm, the channel width was 1 mm and the channel length was 0.6 mm) were deposited on the thin semiconductor films. A triblock copolymer, poly(styreneblock-methyl methacrylate-block styrene) (M_{PMMA} = 11.7 kg/mol, M_W = 19.3 kg/mol, M_{PS} =5.2 kg/mol) and 1-ethyl-3-methylimidazolium bis(trifluoromethylsulfonyl)imide in an ethyl propionate solution were mixed to be ion gel as the dielectric. The polymer films and the gold electrodes were all covered by the prepared ionic solution. A 0.03 mm thick of Al foil was adopted to cover the channels to be the top gate.

Journal Name

View Article Online
DOI: 10.1039/C6RA05709H ARTICLE

Synthesis Procedures.

Synthesis of 1,2-di(thiophen-2-yl)ethyne (1)

2-bromothiophene (3.13 g, 19.20 mmol) and 2-ethynylthiophene (2.17 g, 20.05 mmol) were both dissolved in 200 mL toluene under N_2 atmosphere. After stirring the mixture for 15 min to dissolve the starting materials, 15 mL triethylamine, CuI (0.75 g, 3.97 mmol) and $Pd(PPh_3)_4$ (0.93g, 0.81 mmol) were added into the solution. In the dark environment this reaction solution was kept at 80 °C, stirring constantly for 12 h, then cooled down to room temperature. The resulting mixture was concentrated to dryness, and the crude product was purified through the column chromatography on silica gel to obtain **1** as a white crystal in a yield of 83.2% (3.03 g). ^{1}H NMR (400 MHz, CD_2Cl_2), δ (TMS, ppm): 7.37 – 7.33 (d, 2H), 7.30 – 7.28 (d, 2H), 7.04 – 7.02 (m, 2H); ^{13}C NMR (100 MHz, CD_2Cl_2), δ (TMS, ppm): 132.14, 127.75, 127.22, 85.95. MS (MALDI-TOF): m/z (%): 190.34 (100) [M]. Anal. Calcd for $C_{10}H_6S_2$ (190.28): C, 63.12; H, 3.18; Found: C, 63.37; H, 3.21.

Synthesis of 2,5-bis(thiophen-2-ylethynyl)thiophene (2)

2 was synthesized by the similar procedure as the described for **1** above. 3.58 g 2,5-dibromothiophene (14.79 mmol) and 3.28 g 2-ethynylthiophene (30.33 mmol) were added under N_2 at first. CuI was 0.60 g (3.15 mmol), $Pd(PPh_3)_4$ was 0.67 g (0.58 mmol) and triethylamine was 15 mL. Finally, the product was purified through a column with silica gel to give **2** as dark yellow crystals in a yield of 86.5% (3.79 g). ^{1}H NMR (400 MHz, CD_2Cl_2), δ (TMS, ppm): 7.39 – 7.35 (d, 2H), 7.32 – 7.31 (d, 2H), 7.17 (s, 2H), 7.06 – 7.03 (m, 2H); ^{13}C NMR (100 MHz, CD_2Cl_2), δ (TMS, ppm): 132.60, 132.09, 128.23, 127.34, 124.44, 122.30, 87.38, 85.54. MS (MALDI-TOF): m/z (%): 296.53 (100) [M]. Anal. Calcd for $C_{16}H_8S_3$ (296.43): C, 64.83; H, 2.72; Found: C, 64.92; H, 2.85.

Synthesis of 1,2-bis(5-(thiophen-2-ylethynyl)thiophen-2-yl)ethyne (3)

A flask equipped with a magnetic stirrer was charged with 2-bromo-5-(thiophen-2-ylethynyl)thiophene (2.56 g, 9.51 mmol) coupled with 150 mL toluene. Then CuI (0.21 g, 1.12 mmol), $Pd(PPh_3)_4$ (0.59 g, 0.51 mmol), DBU (20 ml, 0.23 mol), H_2O (147.6 μL, 9.36 mmol) and TMS acetylene (0.60 g, 5.68 mmol) were added. After stirring at 80 °C for 22 h, the mixture was then washed with NH_4Cl solution. The organic layer was then dried over anhydrous $MgSO_4$ and collected by filtration. The mixture was concentrated to dryness. And column chromatography on silica gel provided pure **3** as yellow crystals with a yield of 89.3% (1.71 g). ^{1}H NMR (400 MHz, CD_2Cl_2), δ (TMS, ppm): 7.40 – 7.37 (d, 2H), 7.34 – 7.31 (d, 2H), 7.21 – 7.18 (m, 4H), 7.07 – 7.04 (m, 2H); ^{13}C NMR (100 MHz, CD_2Cl_2), δ (TMS, ppm): 132.66, 132.51, 132.12, 128.30, 127.35, 124.90, 123.94, 122.22, 87.62, 86.86, 85.46. MS (MALDI-TOF): m/z (%): 402.79 (100) [M]. Anal. Calcd for $C_{22}H_{10}S_4$ (402.57): C, 65.64; H, 2.50; Found: C, 65.94; H, 2.63.

Synthesis of 2,5-bis((5-(thiophen-2-ylethynyl)thiophen-2-yl)ethynyl)thiophene (4)

4 was synthesized by the similar procedure as the described for **1** above. 2-bromo-5-(thiophen-2-ylethynyl)thiophene (7.10 g, 26.36 mmol) and 2,5-diethynylthiophene (1.66 g, 12.56 mmol) were added under N_2 at first. CuI was 0.52 g (2.72 mmol), $Pd(PPh_3)_4$ was 0.53 g (0.46 mmol) and triethylamine was 15 mL. Finally, the product was purified through a column with silica gel to give **4** as orange crystals in a yield of 80.2% (5.12 g). ^{1}H NMR (400 MHz, CD_2Cl_2), δ (TMS, ppm): 7.40 – 7.37 (d, 2H), 7.32 – 7.31 (d, 2H), 7.21 – 7.18 (m, 6H), 7.07 – 7.04 (m, 2H); ^{13}C NMR (100 MHz, CD_2Cl_2), δ (TMS, ppm): 132.67, 132.58, 132.55, 132.12, 128.31, 127.35, 124.98, 124.42, 123.87, 87.67, 87.13, 86.80, 85.45. MS (MALDI-TOF): m/z (%): 509.05 (100) [M].Anal. Calcd for $C_{28}H_{12}S_5$ (508.72): C, 66.11; H, 2.38; Found: C, 66.23; H, 2.42.

Polymerization of poly(thienyleneethynylene)s (PTE)

PTE was synthesized by the similar procedure as the described for **1** above. 1.49 g 2,5-diethynylthiophene (11.27 mmol) and 2.79 g 2,5-dibromothiophene (11.53 mmol) were added into 200 mL toluene under N_2. CuI was 0.45 g (2.38 mmol), $Pd(PPh_3)_4$ was 0.48 g (0.42 mmol) and triethylamine was 15 mL. This reaction mixture was stirred at 80 °C for 24 h. In the end, the product was purified through a column with silica gel to give **PTE** as crimson solids in a yield of 64.3% (2.75 g). ^{1}H NMR (400 MHz, CD_2Cl_2), δ (TMS, ppm): 8.15 – 8.04 (m, 1H), 7.24 – 7.20 (m, 1H); Anal. Calcd for C_6H_2S (106.16): C, 67.82; H, 0.02; Found: C, 67.78, H, 0.03.

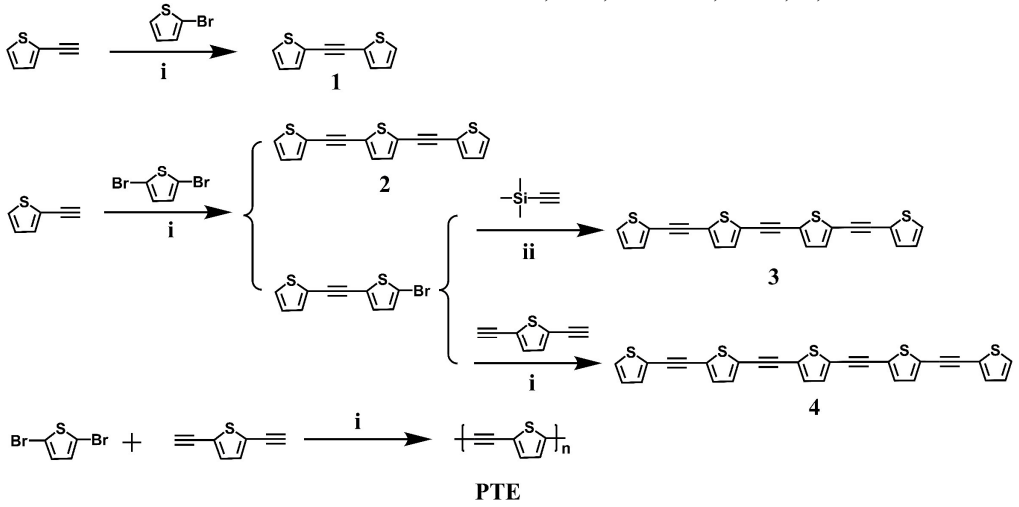

Scheme 1. Procedures for the synthesis of **1-4** and **PTE**. **i**. toluene, triethylamine, CuI, $Pd(PPh_3)_4$, 80 °C; **ii**. toluene, DBU, CuI, $Pd(PPh_3)_4$, H_2O, 80 °C.

View Article Online
DOI: 10.1039/C6RA05709H
Journal Name

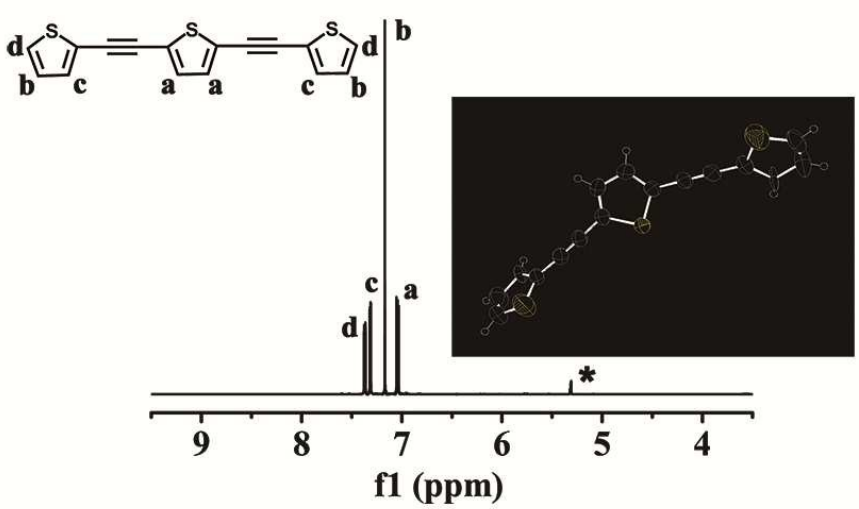

Fig. 1 The ^{1}H NMR spectrum of **2** in CD_2Cl_2, and the signal peak at round 5.3 ppm is attributed to CD_2Cl_2. The inserted picture is ORTEP drawing of **2.**

3. Results and discussions

Synthesis and characterization.

2-Ethynylthiophene and 2,5-diethynylthiophene were synthesized by ourselves referring to some mature methods in the related papers.[32,33] By using the monomers and the Sonogashira coupling reaction,[34] the resulting oligomers **1**-**4** and the polymer **PTE** with good yield were achieved by the synthetic procedures clearly outlined in Scheme 1. All of the pure products were finally obtained by column chromatography on silica gel. Intriguingly, the crystals of **1**-**4** varied from white to orange were recrystallized from their solutions. Luckily, the X-ray crystallographic analysis was used to identify the accurate crystal structure of **2** as the inserted picture in Fig. 1. And its corresponding single-crystal data were collected in Table S1 in the supporting information. ^{1}H NMR is a common and effective method to characterize the products. Herein, ^{1}H NMR spectrum of **2** in CD_2Cl_2 was shown as an example in Fig. 1. In this ^{1}H NMR spectrum, the resonance signals between 7.00 ppm and 7.50 ppm were exactly the characteristic peaks of protons on thiophene. Additionally, the rest oligomers and **PTE** were carefully purified and clearly characterized by solution ^{1}H NMR and ^{13}C NMR, and all of their spectra were displayed in the supporting information (Fig. S1 – Fig. S9). Moreover, the molecular weight of the oligomers could be directly measured by MALDI-TOF, and the mass spectral data of **1**-**4** were also added in the supporting information to affirm their successful synthesis as a further proof (Fig. S10 – Fig. S13).

The elemental polymerization of **PTE** took 24 h in a mild reaction temperature, 80 °C. In fact, there were some red precipitations to appear in the reaction solution at the later stage. In the end of the reaction, some crimson precipitations were separated out from the solution, which portended the possible high molecular weight of the product. Then GPC measurement of the product, with polystyrene as the standard and THF as the eluent (Fig. S14 in the supporting information) was in accordance with the previous anticipation. The number-average molecular weight (M_n) determined of **PTE** was up to 45.0 kg/mol. At the same time, it possessed narrow polydispersity indices (PDIs) of 1.22, which was calculated by means of M_w/M_n. Actually, the high M_n and narrow PDIs are advantages for better film and fiber formation, which are favorable to the later fabrication of FETs.

Thermal properties.

The thermal property of the semiconductor materials is an important factor to form the flexible thin-film FETs. Thus, the thermal measurements of **PTE** were carried out in the N_2 atmosphere. TGA and DSC curves were both shown in Fig. 2. The onset decomposition temperature (the weight of the sample decreased to 95%) of **PTE** was 248 °C, which was assigned to the long and rigid acetylenic structure. Although the thermal stability of **PTE** was inferior to that of the corresponding phenylacetylene-based polymers,[35] the decomposition temperature up to around 250 °C is high enough to be applied in electronic devices. Interestingly, the DSC heating traces of **PTE** in Fig. 2b exhibited its glass-transformation temperature at around 129 °C in the amorphous section. In general, **PTE** possessed good thermal stability because of its well-defined structure containing a long conjugated backbone. The nice thermal property of **PTE** could be vital for achieving the FETs with high performance.

Journal Name
View Article Online
DOI: 10.1039/C6RA05709H
ARTICLE

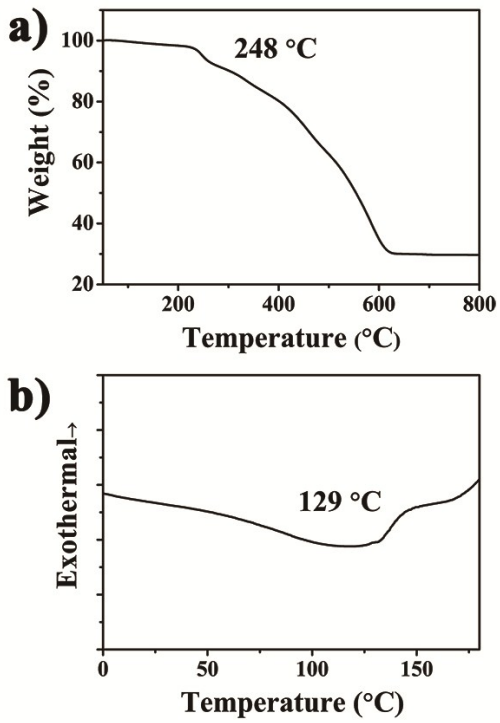

Fig. 2 (a) The TGA curve of **PTE**; (b) The DSC curve of **PTE**.

Optical properties.

Even though the solubility of compounds was becoming worse with the growing length of backbones, they were still dissolved in the organic solvent like CH_2Cl_2. So, all the liquid PL measurements adopted CH_2Cl_2 as the solution of the samples. From Fig. 3a, the upper pictures were the compounds in CH_2Cl_2 solutions under 365 nm UV irradiation. It was clearly observed that the fluorescence of the compounds changed from purple to yellow following a red-shift rule, which could be testified clearly by their PL spectra in the dilute CH_2Cl_2 solution (Fig. 3b). And the corresponding emission wavelengths from 412 nm to 524 nm could be found in Table 1. It was roughly observed by naked eyes that the fluorescent intensity was getting stronger with the longer conjugated backbones, except for the very weak fluorescence of **1**. The effective conjugated length enhanced the extent of the π-electrons of delocalization and narrowed the molecular electronic energy level, which could cause a bathochromic shift in PL emission. But the backbone of **1** was too short to effectively transmit delocalized electrons. Compared to the fluorescence of the compounds in solutions, there was bathochromic shift for the fluorescence of **3**, **4** and **PTE** in their solid state (the lower pictures in Fig. 3a). It was the aggregation of the molecules or molecular chains to lead to the marked bathochromic shift. And Fig. 3c showed the PL spectra of **2**, **3** and **4** in the solid state. The spectra of **1** and **PTE** were not involved, because their fluorescence intensity was too weak to be detected by the instrument. Unlike **1**, **PTE** in solution possessed strong fluorescence while its fluorescence became weakly emissive in the solid state. This is a remarkable phenomenon named aggregation-caused quenching (ACQ), the emissive light of a conventional luminophore is weakened in the condensed state in comparison to them in solution. This is due to the formation of molecular aggregation, which facilitates nonradiative pathways and exciton interactions.[36-38] ACQ appears when the molecular chains of the polymers with certain conjugated degree aggregate more closely in the solid film, so this is the reason that only **PTE** pronouncedly showed this phenomenon. Particularly, parts of molecular chains of **PTE** were able to pack closer by the lamellar and π-π stacking due to the massive thiophene rings and the planarization of the molecular chains. ACQ is a big obstacle to the luminophores, but an advantage for materials applied as a semiconductor. Because there is less energy wasted for emitting light during the process of transmitting electrons. So **PTE** possessed great potential to be applied in electric devices.

Moreover, the detailed UV-vis spectra of the products were displayed in Fig. 3d. Besides the PL emission wavelength in dilute CH_2Cl_2 solution (λ_{em}), the corresponding spectral data like absorption wavelength (λ_{abs}), PL emission wavelength in the condensed state (λ'_{em}), the quantum yields (Φ_F) in dilute CH_2Cl_2 solution using fluorescein (Φ_F = 92% in 0.1M NaOH solution) and quinine sulfate (Φ_F = 54% in 0.1M H_2SO_4 solution) as the references, and fluorescent lifetime (τ) were all collected in **Table 1**. **1-4** and **PTE** possessed absorption wavelengths at 315 nm, 362 nm, 379 nm, 402 nm and 430 nm respectively, resulting in the same red-shift rule with the extended conjugated degree.

Additionally, Φ_F and τ are some other convincing evidences for the former discussion. The data of Φ_F for **1**-**4** and **PTE** in solutions were significantly increasing with the growing backbones, 2.94%, 36.23%, 67.32%, 85.60% and 91.37%. On the other hand, the high efficiency was also attributed to the rigid structure of the backbones. The excited species of the luminescence in solution could relax much more slowly by the restriction of the intramolecular rotations. At the same time, the figure of obtained τ was in the supporting information (Fig. S15). The lifetimes of **1**-**4** were increasing as expected, 0.37 ns, 0.99 ns, 1.02 ns and 1.18 ns. And τ of **PTE** with the high molecular weight was much more than those of the oligomers, perfectly correlating with changes of the growing Φ_F. Unlike the phenomenon in solutions, the Φ_F of **PTE** in the condensed state weakened dramatically. This ACQ phenomenon and its reason have been mentioned before. Even though it was a pity not to collect the PL emission spectrum of **PTE** in the solid state because of its weak fluorescence, it was still clearly observed by naked eyes that the condensed **PTE** emitted crimson fluorescence. This indicated that the PL emission peak of **PTE** in solid must locate in the red range (> 600 nm). This could be explained by the more planar chains of **PTE** to pack closer than that of **1**-**4**. And the small interplanar spacing by means of the strong lamellar and π-π stacking allowed the electrons transfer more easily, resulting in the obvious red-shift phenomenon.

View Article Online
DOI: 10.1039/C6RA05709H
Journal Name

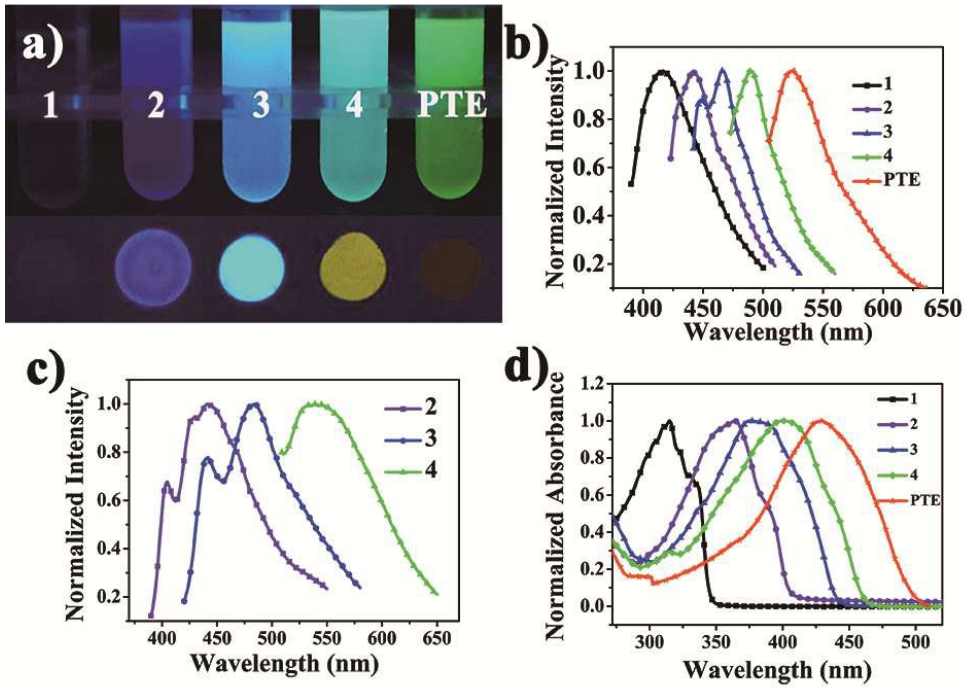

Fig. 3 (a) The upper fluorescent photographs are the compounds in CH_2Cl_2 solutions under 365 nm UV irradiation, and the lower fluorescent pictures are the corresponding solid samples under 365 nm UV irradiation; (b) The normalized PL emission spectra of **1**-**4** and **PTE** in CH_2Cl_2 solutions; (c) The normalized PL emission spectra of **2**, **3** and **4** in solid state; (d) The normalized absorbance spectra of **1**-**4** and **PTE** in CH_2Cl_2 solutions.

Table 1 UV-vis Absorptions and PL Data of **1-4** and **PTE** in CH_2Cl_2 Solution.

Compounds	λ_{abs} [a] (nm)	λ_{em} [b](nm)	λ'_{em} [c](nm)	Φ_F [d] (%)	τ [e] (ns)
1	315	412	-	2.94	0.37
2	362	442	443	36.23	0.99
3	379	466	485	67.32	1.02
4	402	490	541	85.60	1.18
PTE	430	524	-	91.37	1.85

[a] Absorption maximum in dilute CH_2Cl_2 solution. [b] Emission maximum in dilute CH_2Cl_2 solution. [c] Emission maximum in the solid film. [d] Quantum yield estimated with fluorescein (Φ_F = 92% in 0.1 M NaOH) and quinine sulfate (Φ_F = 54% in 0.1M H_2SO_4 solution) as the references. [e] Fluorescent lifetime

Electrochemical properties.

For the sake of an explanation for the pronounced bathochromic-shift fluorescence and figuring out the relationship between the optical features and their intrinsic electronic structures, CV measurements of the resulting compounds were carried out as usual to measure the electrochemical redox behavior of them. The energy band gaps (ΔE_g), the highest occupied molecular orbital (HOMO) and the lowest unoccupied molecular orbital (LUMO) are the most essential parameters in this electrochemical measurement. The original CV curves of **1**-**4** and **PTE** were all arranged in one figure in the supporting information (Fig. S16). Their onset oxidation potential ($E_{onset-ox}$) obtained from CV in acetonitrile could be acquired from these curves. Then, on the basis of the relationships, the HOMO values were always derived from the following classical formulas: HOMO = -e($E_{onset-ox}$-0.0468 V)-4.8 eV (where the value 0.0468 V is for FOC vs Ag/Ag^+), LUMO = ΔE_g + HOMO.

The corresponding data of the compounds, as well as the energy level parameters, were all displayed in Table 2 in turn. The $E_{onset-ox}$ values of **1**-**4** and **PTE** appeared at 0.97, 0.89, 0.51, 0.43 and 0.38 V, respectively. And the values were decreasing in pace with the increasing conjugations as expected. Owing to the $E_{onset-ox}$ values and their oxidation process, the HOMO energy levels of the compounds were estimated to be -5.72, -5.64, -5.26, -5.18 and -5.13 eV in sequence, referring to the former equation. Then PL emission wavelengths in the solutions of compounds were combined with the above data, the final ΔE_g values of all the compounds were calculated to be 2.98, 2.81, 2.66, 2.53 and 2.37 eV, respectively.

Journal Name
View Article Online
DOI: 10.1039/C6RA05709H
ARTICLE

The existing difference in band gaps and HOMO/LUMO values between the oligomers and **PTE** was mainly induced by their different extents of conjugation. The π-extended conjugated backbones formed the main channels for the transmitting electrons. These electrochemical values could meet quite well with the measurements of the compounds in the mentioned optical properties, and were broadly consistent with the incremental molecular conjugation degree. Therefore, these gradually narrowing band gaps with the increasing conjugated backbones fairly demonstrated a strong evidence that a more extended conjugated structure could lower the energy levels for the electronic migration in the conjugated backbones.

Table 2 Electrochemical Properties of **1-4** and **PTE.**

Compounds	E_g (eV)	HOMO (eV)	$E_{onset\text{-}ox}$ (V)	LUMO (eV)
1	2.98	-5.72	0.97	-2.74
2	2.81	-5.64	0.89	-2.83
3	2.66	-5.26	0.51	-2.60
4	2.53	-5.18	0.43	-2.65
PTE	2.37	-5.13	0.38	-2.76

Morphology characterization and 2D-GIXRD.

The crystals of the oligomers were easily recrystallized from their CH_2Cl_2 solution at room temperature. Thus, POM was utilized to study their morphology. It was obvious that **1**-**4** possessed different crystal structures and different fluorescence from Fig. 4, respectively (left pictures were under the room light and the right ones were under UV exposure). Crystal **1** was tiny needle with light blue fluorescence. **2** showed bigger plate-like crystals with a blue light. And **3** owned green thin-plate crystals, plus **4** formed yellow flower-like ones. The oligomers followed the red-shift and the bigger crystal size rules with the increasing backbones. This demonstrated that the growing conjugated degree was a benefit for the ordered aggregation, which was a reason for the strong ACQ phenomenon of **PTE**. In a word, the greater ordered packing morphology was dominant to own better charge-carrier mobility.

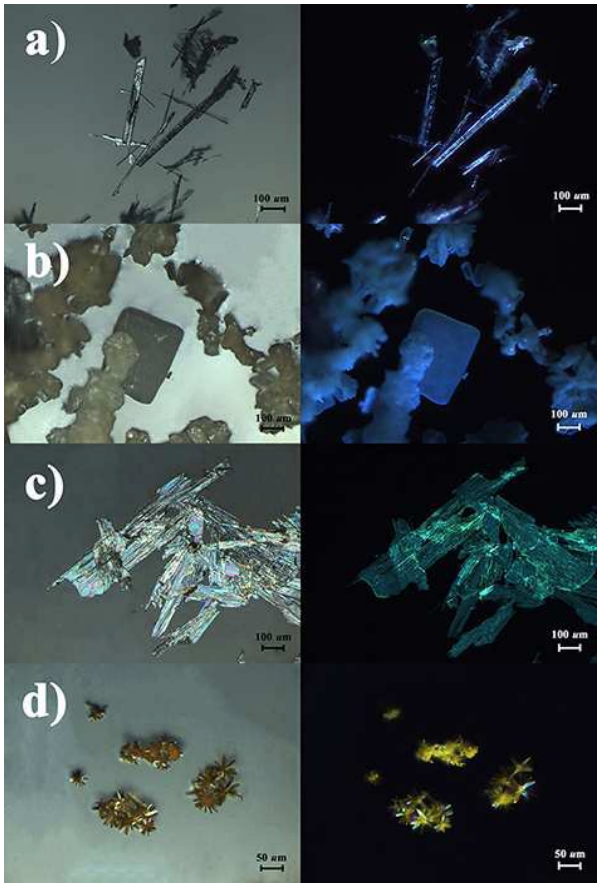

Fig. 4 The POM images under room light on the left and UV exposure on the right of (a)**1**, (b)**2**, (c)**3**, (d)**4**, which were prepared by the slow evaporation of the CH_2Cl_2 solvent at 1 mg/mL.

The packing of the molecules contributes to both the transfer integral and reorganization energy.[39] And the charge carrier mobility in conjugated polymers is mainly dependent on the charge-hopping transport mechanism.[40,41] Hence the morphology and molecular arrangement of semiconducting layers take on significant roles in the charge transport between molecules, which are essential to the performance of FETs.[42-44] Therefore, 2D-GIXRD was employed as an effective technique to analyze the molecular orientation and crystalline structure in thin films of the compounds. The fabricated films were spin-coated on the clean Si/SiO_2 wafers from 0.2 wt % CH_2Cl_2 solutions at room temperature. As the examples, 2D-GIXRD patterns of **3** and **PTE** were displayed in Fig. 5. And the inserted 3D models were schematic diagrams of the molecular packing orientations in their films.

View Article Online
DOI: 10.1039/C6RA05709H
Journal Name

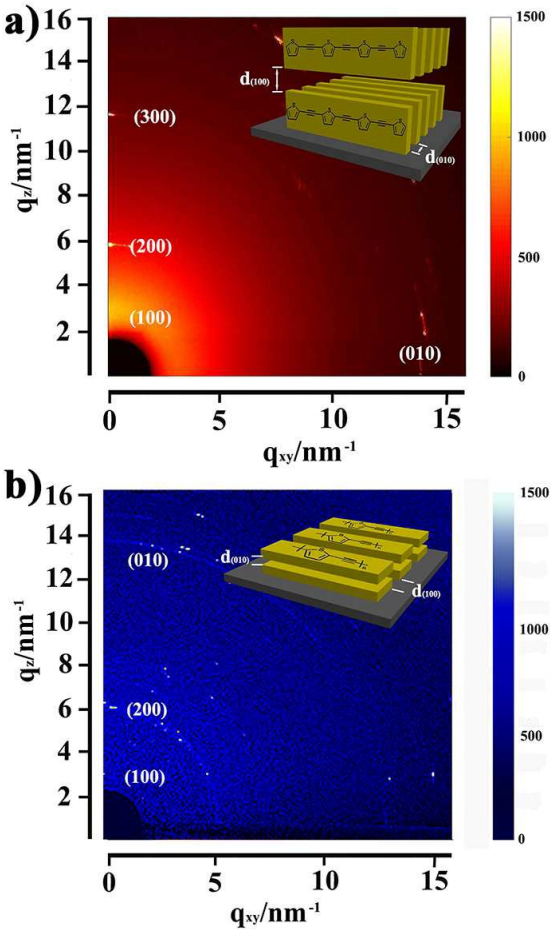

Fig. 5 The 2D-GIXRD patterns of (a) **3** and (b) **PTE**. The insets in (a, b) are schematic diagrams of the orientations of the aggregation structure with respect to the substrate in the films.

The ordered molecular stacking along the direction in the conducting channel is good for charge transport. The 2D-GIXRD study of some thiophene-based compounds like P3HT, showed similar diffraction patterns to our results.[45] Consistently, the (*h*00) and (010) planes reflections indicate along the q_z out-of-plane and q_{xy} in-plane axes, respectively. (*h*00) planes are used as a criterion for the lamellar stacking and (010) reflection is due to the π-π intermolecular stacking.[46-48] As shown in Fig. 5a, the three peaks along the q_z axe were assigned to (100), (200) and (300) diffractions from the lamellar structure, respectively. Simultaneously, the peak on q_{xy} axe was (010) diffraction of the π-π stacking. This diffraction pattern of **3** could be attributed to the edge-on orientation, which was good for carrier conduction along the backbones. And according to the (010) diffraction, the 2D-GIXRD patterns of **PTE** in Fig. 5b showed that there was molecular face-on orientation in the film. As the depiction in the inserted models schematically, this orientation could attenuate the carrier conduction along the π-π stacking direction. The lamellar spacing and the intermolecular spacing of **3** were 2.73 nm and 0.46 nm respectively, according to the (100) plane in this area of q_z = 3.3-3.7 nm^{-1} (out of plane) and the (010) reflection in the area along the q_{xy} = 14.3 nm^{-1} (in plane) axis. Obtained from the diffraction patterns of **PTE**, the d(100) of **PTE** was 2.09 nm at q_z =2.9-3.9 nm^{-1} and its d(010) at q_{xy} = 14.1 nm^{-1} was calculated to 0.44 nm. Probably, there was no steric hindrance caused by side chains to make the spacing of the samples much smaller than some other organic molecules.[49-51] The spacing along the lamellar stacking and the intermolecular stacking of **PTE** were both smaller than those of **3**. This was a further proof of the strong molecular aggregation of **PTE**, which was in accord with the former characterizations. Additionally, the 2D-GIXRD patterns of the rest oligomers **1**, **2** and **4** were arranged in the supporting information (Fig. S17 – Fig. S19). In this system, the lamellar spacing gradually decreased from 3.00, 2.86, 2.73, 2.62 to 2.09 nm for **1**-**4** and **PTE**. The closer molecular stacking was dependent on the increasing conjugated degree.

In general, the 2D-GIXRD results demonstrated that the molecular stacking of compounds **1**-**4** were edge-on orientation with respect to the substrates, and the most molecular chains in **PTE** were stacking with face-on orientation. Actually, they possessed both lamellar stacking and π-π stacking in their thin films. Combined with the other characterizations like PL, the decreasing distance in the lamellar structure with the growing backbones was direct evidence to the stronger molecular aggregation of **PTE** in the condensed state. Thus, this series of compounds were expected to be applied in high performance FETs.

FETs characterization.

Based on the above measurements, the acquired compounds, especially **PTE** with a high conjugated degree, had been proved to possess electronic conductivity and good solubility. This series of compounds showed potential to be a part of some devices like solar cells, diodes, FETs, and so on. Herein, **3** and **4,** selected as the examples of the oligomers, and the polymer **PTE** were used as the semiconductor layer in fabricating FETs to measure their electronic transmission capacity. As one of the most important parts in FETs, the gate dielectric always utilizes some typical inorganic oxides like SiO_2, Al_2O_3 and so on.[52-54] However, it was a fascinating part in our FETs that ion gel was employed to form the gate dielectric layer.[55,56] Notwithstanding, several research groups in the world have manufactured some high-performance FETs with inorganic dielectrics, the organic dielectrics are still in the favourable position because of their prominent features. Besides the remarkable mechanical flexibility just like most of the organic materials, the extraordinarily high capacitance permitting a low voltage operation is another fascinating advantage. A low working voltage is beneficial to decrease the consuming heat in the working devices. So it is an effective way to take advantage of the ion gel as the dielectric combining with the conjugated compounds as the semiconductor to fabricate some possible high-performance FETs.

On the top of Fig. 6, this simple 3D model exhibited the geometric structure of a sort of top-gate FET with the ion gel covered on gold electrodes as the dielectric layer and aluminium as the top gate. The Si/SiO_2 substrates were coated by the selected compounds (**3**, **4** and **PTE**) as the thin-film semiconductor layer via direct solution processing. Besides, there were vapour-deposited gold electrodes between the dielectric and the semiconductor layer. The detailed manufacturing process could be discovered in the former experimental section. Fig. 6a, 6b and 6c were the typical output characteristic curves of the FETs with the samples drop-cast on the substrates, followed by evaporating the surplus solvent in a vacuum environment. The key parameters like drain-source current (I_{DS}) and gate voltage (V_G) characteristics at V_{DS} = 1.0 V could be obtained for these curves. Meanwhile, their transfer characteristic curves and $|I_{DS}|^{1/2}$ versus $|V_G|$ curves of the FETs were depicted in Fig. 6d, 6e and 6f. And the output and transfer curves both distinctly

View Article Online
DOI: 10.1039/C6RA05709H ARTICLE

affirmed that FETs with the organic semiconductor and ion gel emerged p-channel FET characteristics.

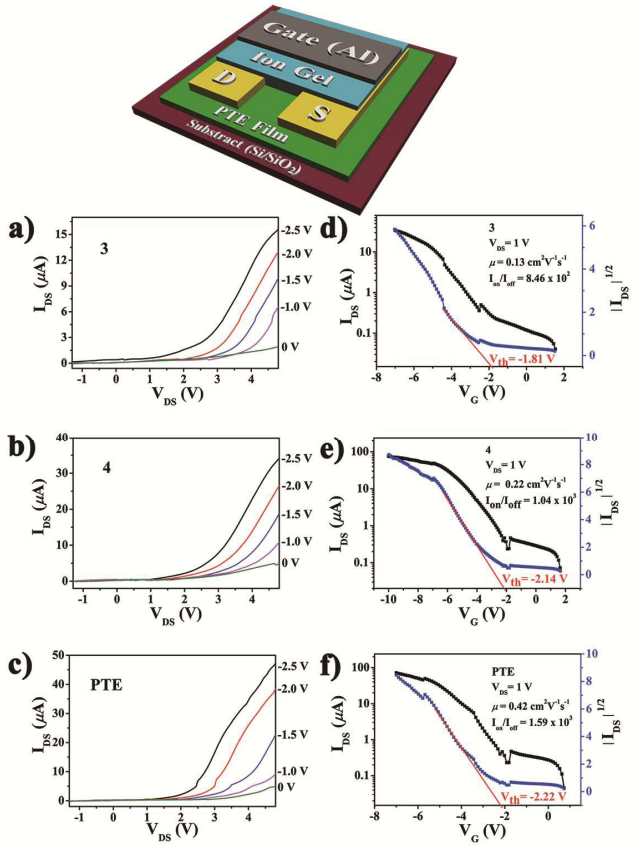

Fig. 6 The 3D model on the top shows the geometric structure of the fabricated top-gate FETs; Output characteristics curves of the FETs consist of (a) **3,** (b) **4** and (c) **PTE**; Transfer characteristic curves at V_{DS} = 1.0 V and the square root of the absolute values of drain current as a function of gate voltage for (a) **3,** (b) **4** and (c) **PTE**. Its calculated charge carrier mobility (μ) maximum values and the on-to-off current ratios (I_{on}/I_{off}) are 0.13 $cm^2V^{-1}s^{-1}$ and 8.46 x 10^2 for **3**; 0.22 $cm^2V^{-1}s^{-1}$ and 1.04 x 10^3 for **4**; 0.42 $cm^2V^{-1}s^{-1}$ and 1.59 x 10^3 for PTE, respectively.

As shown in Fig. 6d, 6e and 6f, a linear relationship within a limited range on the $|I_{DS}|^{1/2}$ versus $|V_G|$ curve obtained at V_{DS} = 1.0 V, the threshold voltages (V_{th}) of FETs involving **3**, **4** and **PTE** were evaluated to -1.81 V, -2.14 V and -2.22 V respectively. In this work, the gate oxide capacitance per unit area of the applied ion gel was 20 $\mu F/cm^2$. From the transfer characteristics, there was a low conductivity at the low V_G, which suggested an excellent air stability thanks to some low HOMO levels of **3**, **4** and **PTE** (-5.26, -5.18 and -5.13 eV). According to the V_{th} values and the transfer characteristics, some μ values were calculated by several groups of I_{DS} and V_G values substituted into the metal-oxide semiconductor FET formula. And the detailed calculations were displayed in the supporting information. In fact, the final μ values of the FETs were picked from several typical results. The figures of the calculated mobility plots versus the related gate voltages for **3, 4** and **PTE** were also placed in the supporting information (Fig. S20). The highest μ value was taken as the adoptive standard. The optimal value of μ for **3** was 0.13 $cm^2V^{-1}s^{-1}$ with a I_{on}/I_{off} of 8.46×10^2, which was not a remarkable performance. Meanwhile, **4** possessed better μ value of 0.22 $cm^2V^{-1}s^{-1}$ with a I_{on}/I_{off} of 1.04×10^3. Compared with the oligomers, **PTE** showed much better performance of 0.42 $cm^2V^{-1}s^{-1}$ with a I_{on}/I_{off} of 1.59×10^3. The extended conjugated degree and the closer aggregation structures had a great influence indeed on the conductive properties according to the above comparisons.

Even if there were lots of FETs with very high mobility values reported in recent years, some of those devices showed quite low I_{on}/I_{off} values even at a high working voltage and some could just work at a very high working voltage.[57-59] The higher working voltage meant to consume more energy to generate useless heat. By compared, **PTE** possessed good thermal and air stability, which was an indispensable condition for stable electronic devices. The nice solubility of **PTE** was propitious to employ simple solution processing. Besides the good mobility with a high enough I_{on}/I_{off} value of the fabricated FETs consisting of **PTE,** they even could work at a low voltage (< 7 V). Low operating voltage was a practical merit for the organic materials to be applied in FETs as well. In short, the good μ and I_{on}/I_{off} of the FETs involving **PTE** meet with its good conducting properties as expected.

4. Conclusions

In summary, a series of oligomers and polymers consisting of alternating thiophene and acetylene units (**1**-**4** and **PTE**) were designed and synthesized via Sonogashira reaction. Then the compounds with different chain lengths were characterized by a lot of routine measurements like ^1H and ^{13}C NMR, MALDI-TOF, UV/vis absorption, PL and CV. The measured results demonstrated not only the successful synthesis of the targeting compounds, but also the influence caused by the growing conjugated backbones on the optical property and electronic conduction. The bathochromic shifts and decreasing band gaps showed the potential nice performance of **PTE** with the longest backbones as the semiconductor layer in FETs. And the π-extended polymer also possessed enough solubility and thermal stability to benefit fabricating thin-film devices. In the actual testing, the FETs involving **PTE** truly owned good performance of μ= 0.42 $cm^2V^{-1}s^{-1}$, which was much better than 0.13 and 0.22 $cm^2V^{-1}s^{-1}$ of those with the selected oligomers (**3** and **4**). Owing to the related measurements, it was clear that the higher molecular weight and more extended conjugated backbone were extraordinarily helpful to the conducting polymers applied in mechanically flexible and high-performance electronic devices.

From the perspective of molecular packing structure adsorbed on surfaces, the employment of 2D-GIXRD was an interesting part to provide a direct explanation for the good performance of **PTE** in this system. The longer conjugated chains of **PTE** resulted in the notably ordered and closer orientation on the surface, which promoted the electronic delocalization quintessential for local charge transports along the π-π stacking direction. It was pronounced that the distance between the molecular lamellar layers of **PTE**, 2.09 nm, was less than those of the oligomers (**1** was 3.00 nm, **2** was 2.86 nm, **3** was 2.73 nm and **4** was 2.62 nm). In a word, this study of the thiophenylethyne-based system indicated the importance of the conjugated backbones and the molecular stacking orientations of the conducting oligo- and polymers. What's more, it showed the potential performance of **PTE** practically applied in the flexible devices like FETs.

Acknowledgements

This work was financially supported by the National Natural Science Foundation of China (21274027 and 20974022) and the Innovation Program of Shanghai Municipal Education

View Article Online
DOI: 10.1039/C6RA05709H
Journal Name

Commission (15ZZ002). The FETs were fabricated and probed in the Micro-Nano Processing and Preparation Public Laboratory, Fudan University. The synchrotron-based 2D-GIXRD measurement was supported by Shanghai Synchrotron Radiation Facility (15ssrf00474).

References

1-59

1 K. Akagi, *Chem. Rev.*, 2009, **109**, 5354-5401.
2 B. Zhu, S. Luo, H. Zhao, H. Lin, J. Sekine, A. Nakao, C. Chen, Y. Yamashita and H. Yu, *Nat. Commun.*, 2014, **5**, 4304-4309.
3 S. Soylemez, S. O. Hacioglu, M. Kesik, H. Unay, A. Cirpan and L. Toppare, *ACS Appl. Mater. Interfaces*, 2014, **6**, 18290-18300.
4 Z. Wang, Q. Liu and B. Ding, *Chem. Mater.*, 2014, **26**, 3364-3367.
5 S. Takamatsu, T. Lonjaret, E. Ismailova, A. Masuda, T. Itoh and G. G. Malliaras, *Adv. Mater.*, 2015, **4**, 249-252.
6 J. Li, S. J. Yoon, B. Hsieh, W. Tai, M. O Donnell and X. Gao, *Nano Lett.*, 2015, **15**, 8217-8222.
7 C. M. Hangarter, N. Chartuprayoon, S. C. Hernández, Y. Choa and N. V. Myung, *Nano Today*, 2013, **8**, 39-55.
8 Z. Chen, J. W. F. To, C. Wang, Z. Lu, N. Liu, A. Chortos, L. Pan, F. Wei, Y. Cui and Z. Bao, *Adv. Energy Mater.*, 2014, **4**, 1400207
9 Q. Zhang, B. Li, S. Huang, H. Nomura, H. Tanaka and C. Adachi, *Nat. Photonics*, 2014, **8**, 326-332.
10 K. Sun, Z. Xiao, S. Lu, W. Zajaczkowski, W. Pisula, E. Hanssen, J. M. White, R. M. Williamson, J. Subbiah, J. Ouyang, A. B. Holmes, W. W. H. Wong and D. J. Jones, *Nat. Commun.*, 2015, **6**, 6013.
11 Z. Wu, L. Chen, J. Liu, K. Parvez, H. Liang, J. Shu, H. Sachdev, R. Graf, X. Feng and K. Müllen, *Adv. Mater.*, 2014, **26**, 1450-1455.
12 X. Guo, J. P. Small, J. E. Klare, Y. Wang, M. S. Purewal, I. W. Tam, B. H. Hong, R. Caldwell, L. Huang, S. O'Brien, J. Yan, R. Breslow, S. J. Wind, J. Hone, P. Kim and C. Nuckolls, Covalently Bridging Gaps in Single-Walled Carbon Nanotubes with Conducting Molecules. Science 2006, **311**, 356-359.
13 X. Jin, D. Sheberla, L. J. W. Shimon and M. Bendikov, *J. Am. Chem. Soc.*, 2014, **136**, 2592-2601.
14 A. Jain and S. J. George, *Mater. Today*, 2015, **18**, 206-214.
15 P. Leclère, M. Surin, P. Viville, R. Lazzaroni, A. F. M. Kilbinger, O. Henze, W. J. Feast, M. Cavallini, F. Biscarini, A. P. H. J. Schenning and E. W. Meijer, *Chem. Mater.*, 2004, **16**, 4452-4466.
16 L. Zhang, N. S. Colella, B. P. Cherniawski, S. C. B. Mannsfeld and A. L. Briseno, *ACS Appl. Mater. Interfaces*, 2014, **6**, 5327-5343.
17 C. B. Nielsen and I. McCulloch, *Prog. Polym. Sci.*, 2013, **38**, 2053-2069.
18 A. M. Glaudell, J. E. Cochran, S. N. Patel and M. L. Chabinyc, *Adv. Energy Mater.*, 2015, **5**, 1401072.
19 H. Yang, T. J. Shin, Z. Bao and C. Y. Ryu, *J. Polym. Sci., Part B: Polym. Phys.*, 2007, **45**, 1303-1312.
20 V. D. Mihailetchi, H. X. Xie, B. de Boer, L. J. A. Koster and P. W. M. Blom, *Adv. Funct. Mater.*, 2006, **16**, 699-708.
21 Q. Liu, Z. Liu, X. Zhang, L. Yang, N. Zhang, G. Pan, S. Yin, Y. Chen and J. Wei, *Adv. Funct. Mater.*, 2009, **19**, 894-904.
22 W. D. Oosterbaan, J. Bolsée, L. Wang, V. Vrindts, L. J. Lutsen, V. Lemaur, D. Beljonne, C. R. McNeill, L. Thomsen, J. V. Manca and D. J. M. Vanderzande, *Adv. Funct. Mater.*, 2014, **24**, 1994-2004.
23 D. L. Trumbo and C. S. Marvel, *J. Polym. Sci., Part A: Polym. Chem.*, 1986, **24**, 2231-2238.
24 F. Chimenti, L. D'Ilario, A. Ettorre, E. Muraglia, G. Ortaggi and G. Sleiter, *J. Mater. Sci. Lett.*, 1992, **11**, 1532-1533.
25 G. V. Tormos, P. N. Nugara, M. V. Lakshmikantham and M. P. Cava, *Synth. Met.*, 1993, **53**, 271-281.
26 H. Hayashi and T. Yamamoto, *Macromolecules*, 1997, **30**, 330-332.
27 M. Iyoda, *C. R. Chim.*, 2009, **12**, 395-402.
28 J. R. Cramer, Y. Ning, C. Shen, A. Nuermaimaiti, F. Besenbacher, T. R. Linderoth and K. V. Gothelf, *Eur. J. Org. Chem.*, 2013, **2013**, 2813-2822.
29 B. McCaughey, C. Costello, D. Wang, J. E. Hampsey, Z. Yang, C. Li, C. J. Brinker and Y. Lu, *Adv. Mater.*, 2003, **15**, 1266-1269.
30 Y. Guo, G. Yu and Y. Liu, *Adv. Mater.*, 2010, **22**, 4427-4447.
31 M. Iyoda, K. Tanaka, H. Shimizu, M. Hasegawa, T. Nishinaga, T. Nishiuchi, Y. Kunugi, T. Ishida, H. Otani, H. Sato, K. Inukai, K. Tahara and Y. Tobe, *J. Am. Chem. Soc.*, 2014, **136**, 2389-2396.
32 S. Uttiya, L. Miozzo, E. M. Fumagalli, S. Bergantin, R. Ruffo, M. Parravicini, A. Papagni, M. Moret and A. Sassella, *J. Mater. Chem. C*, 2014, **2**, 4147-4155.
33 T. X. Neenan and G. M. Whitesides, *J. Org. Chem.*, 1988, **53**, 2489-2496.
34 J. Li and Y. Pang, *Macromolecules*, 1997, **30**, 7487-7492.
35 C. M. Vosloo and A. S. Luyt, *J. Therm. Anal.*, 1995, **44**, 1261-1275.
36 P. Wang, C. J. Collison and L. J. Rothberg, *J. Photochem. Photobiol., A*, 2001, **144**, 63-68.
37 W. Z. Yuan, P. Lu, S. Chen, J. W. Y. Lam, Z. Wang, Y. Liu, H. S. Kwok, Y. Ma and B. Z. Tang, *Adv. Mater.*, 2010, **22**, 2159-2163.
38 N. Zhao, J. W. Y. Lam, H. H. Y. Sung, H. M. Su, I. D. Williams, K. S. Wong and B. Z. Tang, *Chem. Eur. J.*, 2014, **20**, 133-138.
39 J. L. Brédas, J. P. Calbert, D. A. D. S. Filho and J. Cornil, *Proc. Natl. Acad. Sci. U. S. A.*, 2002, **99**, 5804-5809.
40 Z. Chen, P. Müller and T. M. Swager, *Org. Lett.*, 2006, **8**, 273-276.
41 A. Salleo, R. J. Kline, D. M. DeLongchamp and M. L. Chabinyc, *Adv. Mater.*, 2010, **22**, 3812-3838.
42 R. J. Kline, M. D. Mcgehee and M. F. Toney, *Nat. Mater.*, 2006, **5**, 222-228.
43 G. Li, Y. Yao, H. Yang, V. Shrotriya, G. Yang and Y. Yang, *Adv. Funct. Mater.*, 2007, **17**, 1636-1644.
44 J. Dou, Y. Zheng, T. Lei, S. Zhang, Z. Wang, W. Zhang, J. Wang and J. Pei, *Adv. Funct. Mater.*, 2014, **24**, 6270-6278.

Journal Name
View Article Online
DOI: 10.1039/C6RA05709H
ARTICLE

45 S. Joshi, S. Grigorian, U. Pietsch, P. Pingel, A. Zen, D. Neher and U. Scherf, *Macromolecules*, 2008, **41**, 6800-6808.
46 K. E. Aasmundtveit, E. J. Samuelsen, M. Guldstein, C. Steinsland, O. Flornes, C. Fagermo, T. M. Seeberg, L. A. A. Pettersson, O. Inganäs, R. Feidenhans'L and S. Ferrer, *Macromolecules*, 2000, **33**, 3120-3127.
47 T. Lei, Y. Cao, Y. Fan, C. Liu, S. Yuan and J. Pei, *J. Am. Chem. Soc.*, 2011, **133**, 6099-6101.
48 R. Kim, P. S. K. Amegadze, I. Kang, H. Yun, Y. Noh, S. Kwon and Y. Kim, *Adv. Funct. Mater.*, 2013, **23**, 5719-5727.
49 H. Yang, S. W. LeFevre, C. Y. Ryu and Z. Bao, *Appl. Phys. Lett.*, 2007, **90**, 172116.
50 D. H. Kim, B. Lee, H. Moon, H. M. Kang, E. J. Jeong, J. Park, K. Han, S. Lee, B. W. Yoo, B. W. Koo, J. Y. Kim, W. H. Lee, K. Cho, H. A. Becerril and Z. Bao, *J. Am. Chem. Soc.*, 2009, **131**, 6124-6132.
51 H. Liao, C. Tsao, T. Lin, C. Chuang, C. Chen, U. Jeng, C. Su, Y. Chen and W. Su, *J. Am. Chem. Soc.*, 2011, **133**, 13064-13073.
52 L. Liao, J. Bai, Y. Lin, Y. Qu, Y. Huang and X. Duan, *Adv. Mater.*, 2010, **22**, 1941-1945.
53 C. Zhang, Y. Zang, E. Gann, C. R. McNeill, X. Zhu, C. Di and D. Zhu, *J. Am. Chem. Soc.*, 2014, **136**, 16176-16184.
54 J. Huang, J. Pu, C. Hsu, M. Chiu, Z. Juang, Y. Chang, W. Chang, Y. Iwasa, T. Takenobu and L. Li, *ACS Nano*, 2014, **8**, 923-930.
55 S. Lee, B. J. Kim, H. Jang, S. C. Yoon, C. Lee, B. H. Hong, J. A. Rogers, J. H. Cho and J. Ahn, *Nano Lett.*, 2011, **11**, 4642-4646.
56 B. J. Kim, S. Lee, M. S. Kang, J. Ahn and J. H. Cho, *ACS Nano*, 2012, **6**, 8646-8651.
57 X. Liang and S. Wi, *ACS Nano*, 2012, **6**, 9700-9710.
58 G. Lee, Y. Yu, X. Cui, N. Petrone, C. Lee, M. S. Choi, D. Lee, C. Lee, W. J. Yoo, K. Watanabe, T. Taniguchi, C. Nuckolls, P. Kim and J. Hone, *ACS Nano*, 2013, **7**, 7931-7936.
59 X. Wang, F. Zhuang, R. Wang, X. Wang, X. Cao, J. Wang and J. Pei, *J. Am. Chem. Soc.*, 2014, **136**, 3764-3767.

View Article Online
DOI: 10.1039/C6RA05709H
Journal Name

Table of Contents Graphic

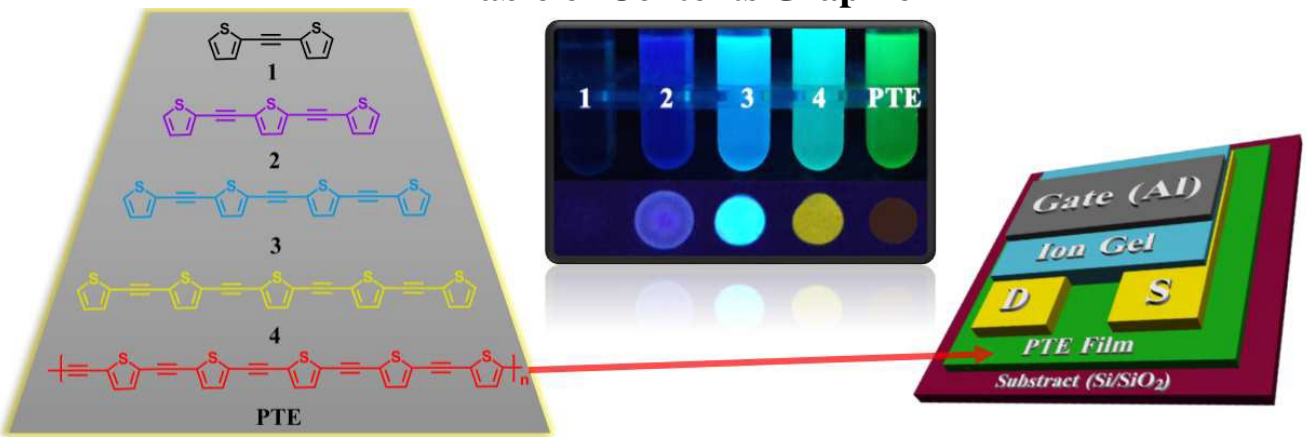

A series of oligomers and polymers consisting of alternating thiophene and acetylene units (**1**-**4** and **PTE**) were designed and synthesized via Sonogashira reaction. And **PTE** was applied as the semiconductor to fabricate FETs with excellent performance. 2D-GIXRD was employed to show the molecular edge-on orientation of **PTE** in the film.